Preparation and Thermal Stability of Gold Nanoparticles in Silk-Templated Porous Filaments of Titania and Zirconia

Junhui He and Toyoki Kunitake*

Frontier Research System, The Institute of Physical and Chemical Research (RIKEN), Hirosawa 2-1, Wako, Saitama 351-0198, Japan

Received March 17, 2004. Revised Manuscript Received April 22, 2004

Porous metal-oxide filaments were readily fabricated using hydrophobic silk as template via the surface sol−gel process, followed by removal of the organic components. Such biotemplated porous matrixes were employed as nanoreactors for in situ synthesis of gold nanoparticles by $NaBH_4$ reduction of the incorporated gold ion. The as-synthesized nanoparticle (ca. 4 nm) was apparently stabilized by the porous morphology of the silk-templated matrix, as well as by the coordinative interaction between the surface Au atom of the nanoparticle with the surrounding oxygen linkage of the matrix. The nanoparticle showed only a small increase (to ca. 6 nm) in particle size after annealing at 500 °C for 5 h, but it became much larger (∼40 nm) at 800 °C. Under the otherwise identical conditions, amorphous zirconia matrix gave rise to a much smaller size increase (ca. 10 nm at 800 °C), indicating more effective suppression of fusion of molten gold nanoparticles. Apparently, better physical isolation of the nanoparticle was attained for amorphous zirconia than nanocrystalline titania. General features of the formation of metal nanoparticles in solid matrixes were discussed, in terms of morphology and functionality of matrixes.

Introduction

Fabrication of metallic and semiconductor nanoparticles deposited in inorganic porous materials is attracting increasing interest in terms of practical applications and synthetic challenges. For example, effective optical gas sensing was achieved by embedding semiconductor nanoparticles in porous siliceous MCM-41.[1] Mesoporous silica and zirconia that contained metal or semiconductor nanoparticles were studied for nonlinear optical properties,[2] and those with γ-Fe_2O_3 nanoparticles were fabricated as advanced magnetic materials.[3] Other important applications include heterogeneous catalysts[4] and microwave absorbing materials.[5]

Inorganic porous matrixes are usually produced by the sol−gel process using structure-directing agents such as surfactants. Nanoparticles are embedded either by simultaneous in situ synthesis or by impregnation of preformed nanoparticles. Fascinating, versatile biological structures, many of which are porous, provide unique templates for such porous structures. Replication of bacteria and wood cell by inorganic materials has given zeolitic materials of high porosity.[6] However, such biotemplated porous matrixes have never been used for in situ formation of nanoparticles.

Spider silk was previously used for biomimetic synthesis of functional composites by coating with colloidal magnetite, CdS, and gold particles, and for synthesis of hierarchically ordered hollow mesoporous silica fibers by applying a liquid-crystalline silica−surfactant mesophase.[7] Silk consists of fibroin protein, and this is spun mechanically by silkworm to aligned polypeptide chains (including crystalline and amorphous domains). Fibroin mainly contains amino acids with short side chains such as glycine, alanine, and serine (more than 80% when tyrosine is included) and those with polar side chains occur only in small amounts.[8] Silk filaments have a smooth surface and significant porosity. The specific surface area was estimated to be 250 m^2/g.[9] The excellent absorption and desorption properties provide a microclimate comfortable for the human body and thus make silk a widely used, excellent fiber for textiles. It is interesting if the exquisite morphology of silk fibers is used in fabrication of novel functional materials. Unfortunately, the hydrophilic components that are

* To whom correspondence should be addressed. E-mail: kunitake@ruby.ocn.ne.jp.

(1) Wark, M.; Rohlfing, Y.; Altindag, Y.; Wellmann, H. *Phys. Chem. Chem. Phys.* **2003**, *5*, 5188−5194.

(2) (a) Govindaraj, R.; Kesavamoorthy, R.; Mythili, R.; Viswanathan, B. *J. Appl. Phys.* **2001**, *90*, 958−963. (b) Haus, J. W.; Kalyaniwalla, N.; Inguva, R.; Bloemer, M.; Bowden, C. M. *J. Opt. Soc. Am. B* **1989**, *6*, 797−807. (c) Tanaka, A.; Onari, S.; Arai, T. *Phys. Rev. B* **1993**, *47*, 1237−1243.

(3) Solinas, S.; Piccaluga, G.; Morales, M. P.; Serna, C. J. *Acta Mater.* **2001**, *49*, 2805−2811.

(4) (a) Bell, A. T. *Science* **2003**, *299*, 1688−1691. (b) Rolison, D. R. *Science* **2003**, *299*, 1698−1701.

(5) Vendange, V.; Tronc, E.; Colomban, Ph. *J. Sol-Gel Sci., Technol.* **1998**, *11*, 299−307.

(6) (a) Davis, S. A.; Burkett, S. L.; Mendelson, N. H.; Mann, S. *Nature* **1997**, *385*, 420−423. (b) Dong, A.; Wang, Y.; Tang, Y.; Ren, N.; Zhang, Y.; Yue, Y.; Gao, Z. *Adv. Mater.* **2002**, *14*, 926−929.

(7) (a) Mayes, E. L.; Vollrath, F.; Mann, S. *Adv. Mater.* **1998**, *10*, 801−805. (b) Huang, L.; Wang, H.; Hayashi, C. Y.; Tian, B.; Zhao, D.; Yan, Y. *J. Mater. Chem.* **2003**, *13*, 666−668.

(8) Salamone, J. C., Ed. *Polymeric Materials Encyclopedia*, *Vol. 10*; CRC Press: Boca Raton, FL, 1996; pp 7711−7719.

(9) Borovskii, V. R.; Shelimanov, V. A.; Bykova, G. P. *Teplofiz. Teplotekh.* **1973**, *25*, 50−52.

10.1021/cm049548l CCC: $27.50
Published on Web 05/26/2004

often employed for coating spider silk may not fully reach and faithfully replicate all of its structural details because silk is a highly hydrophobic, insoluble biopolymer.

We developed the surface sol−gel process as a novel method of fabricating metal-oxide ultrathin films.[10] It is based on adsorption of metal-alkoxide molecules from solution onto hydroxylated surfaces and subsequent hydrolysis to give nanometer-thick oxide films. The film thickness can be adjusted to molecular precision by choosing appropriate fabrication conditions, and functionalization of such thin films is realized by incorporation of metal ions that leads to in situ synthesis of mono- and bimetallic nanoparticles.[11−14] We also applied this process to curved surfaces such as those of latex particles, tobacco mosaic virus, and cellulose fibers to produce hollow spheres and tubular structures.[15,16] In all these cases, substrates and templates possessed hydrophilic, polyhydroxylated surfaces to allow their facile reaction with metal alkoxides in solution. This approach would be much expanded if we can employ hydrophobic functional surfaces. This possibility was tested in the current study by using hydrophobic silk fibers.

The stability of nanoparticles is another important issue of particle/matrix composites, as aggregation of nanoparticles will lead to deterioration of their functionalities. It is known that nanoparticles are stabilized under ambient conditions by porous morphology of the matrix[17] and by interaction with the matrix.[14,17,18] In contrast, their high-temperature stabilities have been hardly examined, despite its significance in automobile catalysis and other practical applications. Therefore, we studied here thermal behavior of gold nanoparticles embedded in silk-templated porous metal oxides.

Experimental Section

Silk threads were purchased from Kanebo (Japan). Ti(O*n*Bu)$_4$ and Zr(O*n*Bu)$_4$ were obtained from Gelest. $NaBH_4$ and $AuCl_3$ were purchased from Kanto Chemical and Aldrich, respectively. All these chemicals were guaranteed reagents and used as purchased. Ultrapure water with a specific resistance of 18.3 MΩ·cm was obtained by reverse osmosis followed by ion exchange and filtration (Yamato-WQ500, Millipore, Japan).

Silk threads are composed of silk filaments and were used as the template for the surface sol−gel process. Ti(O*n*Bu)$_4$ and Zr(O*n*Bu)$_4$ in toluene (100 mM) were used as precursor solutions. In a typical procedure, silk threads were first immersed in a precursor solution for 10 min. After rinsing twice with toluene (each for 1 min), silk threads were sucked dry on a filtering unit and left in air for hydrolysis by moisture. These steps constitute 1 cycle and 10 cycles were repeated. Then, the silk/metal-oxide composite threads were dried in vacuum overnight. They were finally heated at a rate of 1 K/min from room temperature to 450 °C and calcined at this temperature for 4 h to remove the organic components.

A piece of the metal-oxide thread was immersed in aqueous $AuCl_3$ (10 mM) for 1 min. After being rinsed in ethanol for 30 s, it was placed in aqueous $NaBH_4$ (200 mM) for 10 min, the Au^{3+} ions being reduced to Au nanoparticles. Finally, it was rinsed in pure water for 1 min and dried in vacuum overnight.

Scanning electron microscopy (SEM) and transmission electron microscopy (TEM) observations were carried out on an Hitachi S-5200 field emission scanning electron microscope and a JEOL JEM-2000EX transmission electron microscope, respectively. Titania filaments were observed directly by SEM without metal coating, while those of zirconia were coated with 2 nm of Pt by an Hitachi E-1030 ion coater before observation. The histogram, mean diameter, and standard deviation of nanoparticles were obtained by sampling 100 metal nanoparticles in TEM images of 3×10^5 magnification, followed by analyses using SigmaPlot 2001.

Results

1. Replication of Silk Filament Morphology by Titania. The inset in Figure 1a shows free-standing, light-yellow titania threads fabricated using Ti(O*n*Bu)$_4$ (100 mM) as the precursor solution. Small shrinkage was noticed compared with the original silk thread. A piece of the sample was observed without metal coating on FE-SEM. As shown in Figure 1a, bundles of spongy titania filaments were observed. The width of the filament was ca. 5 μm, and smaller than that (ca. 9 μm) of the original silk filament, in agreement with the above-mentioned macroscopic shrinkage. Magnified images (Figure 1b−d) show that the titania filaments are in fact hierarchically porous. The large pores are ca. 100 nm in diameter. The small pores are less than 10 nm in diameter and located in the wall of the large pores. Thus, the highly porous character of silk was effectively inherited by the titania filament. These titania morphologies are remarkably different from those derived from cellulose as the template.[16] It is interesting that a helical structure was also observed (Figure 1e). As fibroin crystals consist of molecular chains with a helical conformation,[8] the observation of the helical titania structure is not surprising.

The titania filament was also observed by TEM. A piece of the titania thread was placed in a small vial and a small amount of pure water was added. After sonication, it was transferred onto a SiO-coated copper grid and dried overnight. TEM observations were carried out at 120 kV. Figure 2 shows TEM images of a titania filament at both low (Figure 2a) and high (Figure 2b) magnifications. The filament looks spongy and has a width of ca. 2 μm (Figure 2a). Clearly, nanopores (≤10 nm) (Figure 2b) were formed in the titania filaments. The selected area electron diffraction (SAED) pattern (Figure 2b, insert) indicates that the filaments consist of well-crystallized anatase.

2. Preparation and Thermal Stability of Gold Nanoparticles. Recently, we reported facile in situ synthesis of noble metal nanoparticles in porous cellulose fibers.[17] The nanoporous structure and the high density of oxygen linkage in the cellulose fiber constituted an effective nanoreactor for the in situ synthesis. The nanopore is essential for efficient incorporation of metal ion and reductant into cellulose fibers as well as

(10) Ichinose, I.; Senzu, H.; Kunitake, T. *Chem. Lett.* **1996**, 831−832.
(11) He, J.; Ichinose, I.; Fujikawa, S.; Kunitake, T.; Nakao, A. *Chem. Mater.* **2002**, *14*, 3493−3500.
(12) He, J.; Ichinose, I.; Kunitake, T.; Nakao, A. *Langmuir* **2002**, *18*, 10005−10010.
(13) He, J.; Ichinose, I.; Fujikawa, S.; Kunitake, T.; Nakao, A. *Chem. Commun.* **2002**, 1910−1911.
(14) He, J.; Ichinose, I.; Kunitake, T.; Nakao, A.; Shiraishi, Y.; Toshima, N. *J. Am. Chem. Soc.* **2003**, *125*, 11034−11040.
(15) Fujikawa, S.; Kunitake, T. *Langmuir* **2003**, *19*, 6545−6552.
(16) Huang, J.; Kunitake, T. *J. Am. Chem. Soc.* **2003**, *125*, 11833−11834.
(17) He, J.; Kunitake, T.; Nakao, A. *Chem. Mater.* **2003**, *15*, 4401−4406.
(18) Franke, R.; Rothe, J.; Pollmann, J.; Hormes, J.; Boennemann, H.; Brijoux, W.; Hindenburg, Th. *J. Am. Chem. Soc.* **1996**, *118*, 12090−12097.

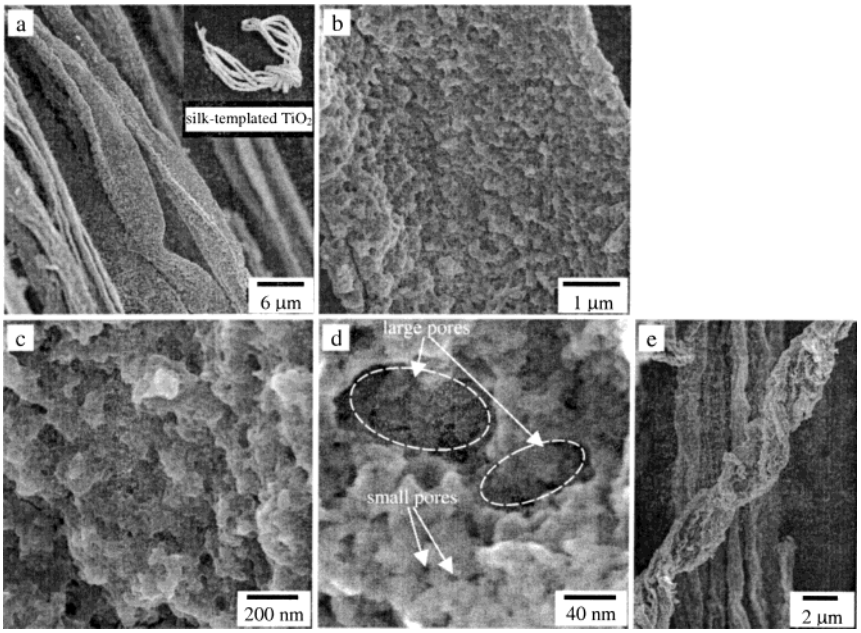

Figure 1. SEM images of (a) tatania filaments, (b)−(d) single filament at higher magnifications, and (e) titania helix. Insert in (a): photo of silk-templated titania.

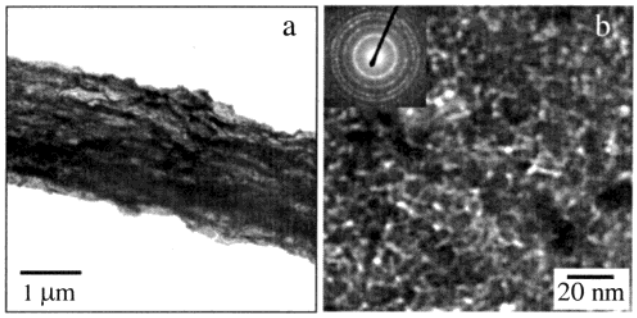

Figure 2. TEM images of titania filaments at low (a) and high (b) magnifications. Insert in (b): SAED pattern.

for removal of unnecessary byproducts from fibers. The spongy titania filament obtained in the present work provides a similar environment.

As shown in Figure 3a, as-synthesized Au nanoparticles in the titania filament are small, and their mean diameter and standard deviation are estimated to be 3.9 nm (d) and 1.2 nm (σ), respectively. After the composite was annealed at 500 °C for 5 h, the nanoparticle size increased to 6.2 nm, though the size distribution remained almost unchanged ($\sigma = 1.3$ nm) (Figure 3b). Further annealing of the composite at 800 °C for 5 h resulted in a significant increase in particle size and size distribution, the mean diameter and standard deviation being 40.4 and 14.4 nm, respectively (Figure 3c). Figure 3d shows their temperature dependence. It is clear that significant increases in particle size and size distribution occur only at temperatures over 500 °C. The inset in Figure 3d is a schematic illustration of the annealing process, which represents the size increase of Au nanoparticles in titania filaments.

Further details of the particle growth were revealed by a magnified TEM image of Figure 4. After the sequential annealing at 500 and 800 °C, the Au/TiO_2 composite is in fact composed of both Au nanoparticles and TiO_2 nanocrystals. Those Au nanoparticles located within pores are apparently confined by the pores

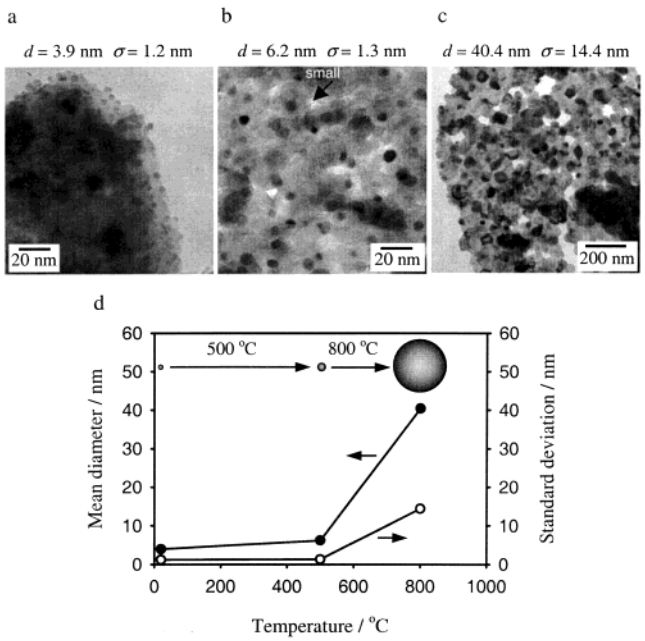

Figure 3. TEM images of Au nanoparticles in porous titania filaments (a) as-prepared, (b) after annealing at 500 °C for 5 h (the arrow pointing to a small pore), (c) after additional annealing at 800 °C for 5 h, and (d) temperature dependence of particle mean diameter (●) and standard deviation (○). Insert in (d): schematic illustration of annealing in which the diameters of the spheres are in the ratios of particle mean diameters.

(interstices) formed by TiO_2 crystals and cannot grow beyond the size of the pore (note both the size and shape of such Au nanoparticles and the corresponding pore, as indicated by solid arrows in Figure 4). In contrast, Au nanoparticles that are not confined in the pore may grow to much larger particles (as pointed out by a dashed arrow). The coexistence of different growth mechanisms (confined and unconfined) eventually results in a wider size distribution of Au nanopaticles in titania filaments.

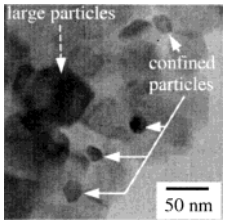

Figure 4. TEM image of Au nanoparticles in porous titania filaments after sequential annealing at 500 °C for 5 h and then at 800 °C for 5 h. The solid arrows point to confined Au particles and the dashed arrow points to a larger Au particle.

The above discussion is supported by taking into account the melting point (mp) of Au nanoparticles. The melting point is estimated from the reported dependence of melting point on particle size.[19] It is ca. 700 °C for the as-synthesized Au nanoparticle of $d = 3.9$ nm and ca. 740 °C for the Au nanoparticle of $d = 6.2$ nm (as obtained by annealing at 500 °C). Apparently, the as-synthesized Au nanoparticle did not melt during annealing at 500 °C, in agreement with the small change in particle size. In contrast, the annealing temperature of 800 °C is higher than the melting point of Au nanoparticle of $d = 6.2$ nm; thus, heating at 800 °C must have led to melting of the Au nanoparticle. It is conceivable that such melted Au nanoparticles migrate and fuse more readily with neighboring particles, leading to the significant increase in the particle size.

As commonly observed,[20] titania crystals also grew significantly by annealing at 800 °C (compare Figure 3c and Figure 4 with parts (a) and (b) in Figure 3). Such crystal growth may exclude the embedded melted gold nanoparticles, leading to their fusion and the formation of large particles.

3. Thermal Stability of Gold Nanoparticles in Silk-Templated Amorphous Zirconia Filaments. To clarify the role of the matrix morphology in the nanoparticle stability, zirconia, an amorphous metal oxide,[21] was chosen as a second matrix for in situ synthesis of Au nanoparticles. Hierachically porous zirconia filaments were fabricated in a procedure similar to that of titania, and in situ synthesis of Au nanoparticles was conducted under identical conditions. The as-prepared Au nanoparticle has almost the same mean diameter ($d = 4.1$ nm) and standard deviation ($\sigma = 1.0$ nm) (Figure 5a) as those in titania (Figure 3a). After annealing at 500 °C for 5 h, the size and its distribution increased only slightly ($d = 5.0$ nm and $\sigma = 1.4$ nm) (Figure 5b). Further annealing at 800 °C resulted in larger increases in the size and size distribution ($d = 10.9$ nm and $\sigma = 4.3$ nm) (Figure 5c). However, the size increase at 800 °C is much smaller than that observed in the titania matrix. In other words, the Au nanoparticles embedded in amorphous zirconia are much more stable than those in crystalline titania at 800 °C. This is not surprising, if we consider that the structure of amorphous zirconia does not change much at 800 °C because this temperature is far below its melting point, 2710 °C.[21] In contrast, crystal growth proceeds at 800

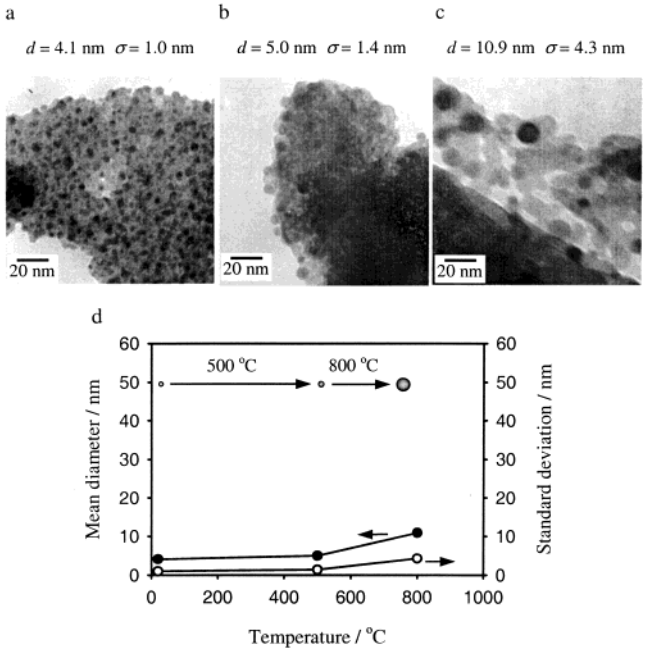

Figure 5. TEM images of Au nanoparticles in porous zirconia filaments (a) as-prepared, (b) after annealing at 500 °C for 5 h, (c) after additional annealing at 800 °C for 5 h, and (d) temperature dependence of particle mean diameter (●) and standard deviation (○). Insert in (d): schematic illustration of annealing in which the diameters of the spheres are in the ratios of particle mean diameters.

°C for titania, and it may cause exclusion of molten Au nanoparticles, leading to their fusion to much larger particles. Figure 5d shows the temperature dependence of mean diameter and standard deviation of Au nanoparticles in zirconia. Clearly, the temperature dependence in amorphous zirconia is less significant compared with that observed in crystalline titania (Figure 3d).

Discussion

1. Surface Sol−Gel Process on a Hydrophobic Surface. Templates and substrates suitable for the surface sol−gel process usually have hydrophilic, polyhydroxylated surfaces to allow their surface reaction with metal alkoxides in solution (Scheme 1a). Although silk consists of a large number of peptide-derived amino and hydroxyl groups,[8] its fiber is highly hydrophobic and insoluble.[6] This fiber property is created by strong cooperative hydrogen bonding between polypeptide chains.[22] In fact, silk is less hygroscopic than cotton. However, if metal alkoxides are dissolved in nonpolar solvents, they can reach surfaces, inner pores, and amorphous domains of silk microfibrils and will react with surface-functional units of fibroin. The lysine, histidine, and tyrosine units provide reactive side chains, as shown in Scheme 1b. Further reaction would produce composite fibers of silk and metal-oxide gel. Our experimental results prove that hierarchically porous metal-oxide filaments are produced upon removal of organic components by calcination, replicating the exquisite morphology of silk. Clearly, the surface sol−gel process is effective not only for hydrophilic, polyhydroxylated surfaces but also for functional, hydrophobic

(19) Buffat, Ph.; Borel, J.-P. *Phys. Rev. A* **1976**, *13*, 2287−2297.
(20) Möckel, H.; Giersig, M.; Willig F. *J. Mater. Chem.* **1999**, *9*, 3051−3056.
(21) Lide, D. R.; Ed, *CRC Handbook of Chemistry and Physics*, 81st ed.; CRC Press LLC: Boca Raton, FL, 2000; pp 4−100.
(22) Lele, A. K.; Joshi, Y. M.; Mashelkar, R. A. *Chem. Eng. Sci.* **2001**, *56*, 5793−5800.

Scheme 1. (A) Schematic Illustration of the Surface Sol−Gel Process; (B) Reaction of Silk Fibroin with Metal Alkoxide

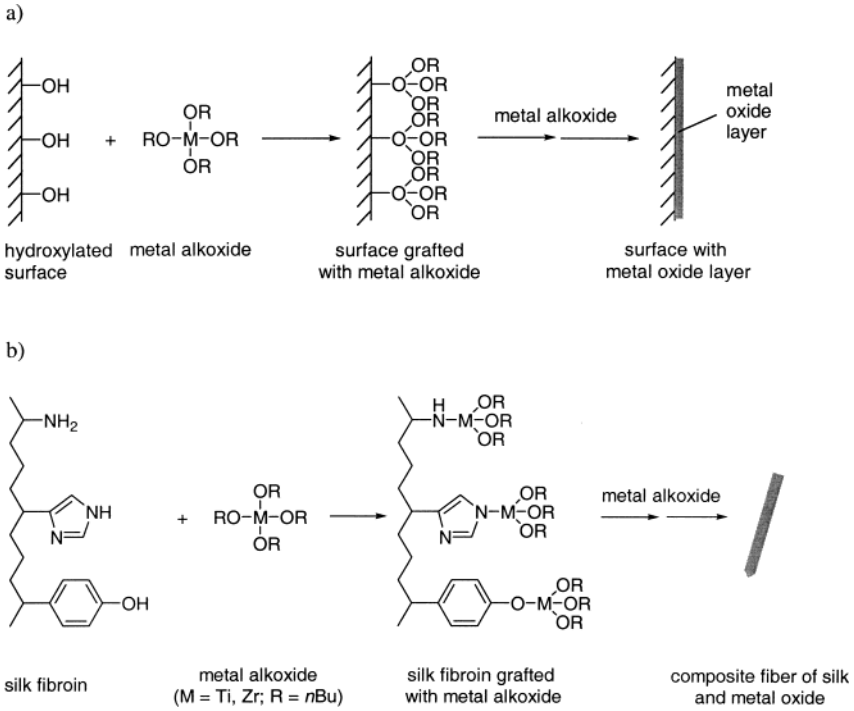

Table 1. Matrix Characteristics and Au Ion Incorporation

	original matrix	metal-oxide replica
cellulose-based	porous fiber, hydrophilic, wettable by aqueous solution, homogeneous incorporation of metal ions	porous tubule, hydrophilic, polycrystalline and amorphous, wettable by aqueous solution, homogeneous incorporation of metal ions
silk-based	porous fiber, hydrophobic, wettable by nonpolar solution, inhomogeneous adsorption of metal ions	porous strand, hydrophilic, polycrystalline and amorphous, wettable by aqueous solution, homogeneous incorporation of metal ions

surfaces. The usefulness of the surface sol−gel process is, thus, much extended.

2. In Situ Synthesis of Au Nanoparticles in Natural Fibers and in Their Metal-Oxide Replicas. Matrix-mediated fabrication of metal nanoparticles consists of two basic processes of metal ion incorporation and in situ reduction. The second step does not appear to be influenced by the nature of the matrixes, while the incorporation process is decisive. Two major factors that affect efficiency of metal ion incorporation will be morphology and functional property of a given matrix. The matrixes we have employed in our studies are fibers of cellulose and silk and their metal-oxide replicas (Table 1).

Cellulose fiber is porous and hydrophilic. It is highly wettable by aqueous solution. Its nanoporous structure and a high density of the oxygen linkage allows efficient, homogeneous incorporation of metal ions, acting as an effective nanoreactor for in situ synthesis of metal nanoparticles. The produced metal nanoparticles are homogeneously distributed in the cellulose fiber, as indicated by the uniform color of the composite.[17] On the other hand, silk fiber is porous, but is highly hydrophobic, and aqueous $AgNO_3$ cannot effectively wet silk filaments. This causes inhomogeneous adsorption of a small amount of Ag^+ ions after rinsing. In situ reduction under identical conditions only gives silver nanoparticles (ca. 3 nm in diameter) inhomogeneously distributed on silk filaments, and the composite is not uniformly colored.

Replication of silk to porous strands by the surface sol−gel process was possible only when alkoxides were dissolved in nonpolar solvents. The hydrophobic silk fiber is wettable by nonpolar solution. The obtained titania replicas are polycrystalline, while the zirconia replicas are amorphous. Both of them are hydrophilic and wettable by aqueous solution.[11−14] Thus, metal ions are readily incorporated in these porous replicas and are converted to metal nanoparticles by in situ reduction.

3. Thermal Stability of Gold Nanoparticles in Metal-Oxide Matrixes. The stability of metal nanoparticles at high temperatures is attributed to the porous morphology of the ceramic matrix and to the strong bonding interaction between the surface atom of the nanoparticle and the surrounding oxygen linkage of the matrix.[14,18] This is the case even with an organic matrix such as cellulose.[17] A second important factor is melting points of metal nanoparticles. The melting point of metals is size-dependent at the nanometer scale and becomes lower with a decrease in particle size.[19] As described in the Results, melting of nanoparticles will promote their fusion to induce large increases in particle size and its distribution. However, the fusion may be retarded if individual nanoparticles are physically isolated from each other. Thus, the physical form of the ceramic matrix should be considered as a third factor

that affects thermal stability of metal nanoparticles. Zirconia is an amorphous matrix and its morphology does not change much with increasing temperature in the temperature range below its melting point (2710 °C). In contrast, amorphous titania prepared by the sol−gel process crystallizes to form anatase and rutile at different temperatures. According to our results, amorphous zirconia was more effective for stabilizing embedded metal nanoparticles than crystalline titania. The difference of the two matrixes is much enhanced at 800 °C than at 500 °C. The gold nanoparticle of 4−6 nm is estimated to become molten at 700−740 °C (vide ante), and it must be completely molten at 800 °C. It was reported that gold nanoparticles (6 ± 1 nm) on a carbon nanotube underwent fusion after heating for 30 s at 300 °C.[23] The effectiveness of the amorphous zirconia to suppress extensive fusion at this temperature suggests that the molten nanoparticles are totally buried in the metal-oxide network of amorphous zirconia, being physically isolated from the neighboring nanoparticles. In contrast, the nanocrystalline titania matrix was less effective for suppressing the fusion, especially at 800 °C. Apparently, the nanoparticle becomes exposed at least partially during growth of the anatase nanocrystal at elevated temperatures. The exposed nanoparticle would fuse more readily. It is clear that the stability of metal nanoparticles can be much enhanced by utilization of a matrix that can keep its amorphous morphology at elevated temperatures. The current results point to better design and more appropriate application of heterogeneous catalysts.

4. Direct vs Indirect Incorporation of Metal Nanoparticles into Solid Matrixes by Chemical Means. Composites of metal nanoparticles in solid matrixes can be fabricated either by incorporation of preformed nanoparticles or by in situ formation of nanoparticles. In the case of direct incorporation, colloidal metal nanoparticles are usually synthesized in solution and stabilized by thiol compounds, polymers, surfactants, and other protecting ligands. Undoubtedly, the nature of the organic protecting shell will strongly affect physicochemical properties (e.g., catalytic properties) of metal nanoparticles and their ease of impregnation in solid matrixes. On the other hand, the in situ formation is composed of incorporation of metal ions and subsequent reduction to nanoparticles. There are two different ways of efficient incorporation. One is the ion-exchange approach and the other is the coordination approach. Baumann and co-workers prepared ion-exchangeable K^+-doped organic hydrogel in the void of a 3D ordered array of PS spheres, from which composites of metal nanoparticles in ordered macroporous carbons were produced.[24] Recently, we developed a general way of incorporation of metal ions in ultrathin metal-oxide films by an ion-exchange process.[11] This method is quite flexible, and the amount of incorporated metal ions is readily altered by adjusting the number of ion-exchange sites. In contrast, the results described in the present article belong to a typical case of the coordination approach. Metal-oxide replicas of cellulose and silk provide porous matrixes with highly populated oxygen linkages. Coordination of noble metal ions to densely populated oxygen units must be effective for trapping the metal ion. Cellulose fibers can also provide efficient sites of metal ion incorporation, as we recently described.[17] Although the metal-oxide film and cellulose fibers are totally different matrixes, they have common features such as porous morphology and high density of oxygen linkage (see Table 1). These structural characteristics are apparently responsible for efficient incorporation of metal ions as well as for stabilization of in situ converted metal nanoparticles. The in situ approach should be extendable to fabrication of a wide variety of other nanoparticle/matrix composites.

Conclusion

We can conclude from the current study that highly porous structures of metal oxides as templated by natural fibers are superior matrixes for stably accommodating gold nanoparticles. It is important to note that the nanoparticles do not essentially fuse even at temperatures higher than their melting points when physically isolated in metal-oxide networks. This conclusion should be extended to other metal nanoparticles. It is clear that physical isolation is a most influential factor for high-temperature stabilization.

Acknowledgment. We are very grateful to Ms. Rie Takagi for her technical support with TEM measurements.

CM049548L

(23) Fullam, S.; Cottel, D.; Rensmo, H.; Fitzmaurice, D. *Adv. Mater.* **2000**, *12*, 1430−1432.

(24) Baumann, T. F.; Satcher, J. H. Jr. *Chem. Mater.* **2003**, *15*, 3745−3747.